**Please Note:** Changes were made to this manuscript in the final proof and publication stage. Please consult the Version of Record (<a href="https://www.doi.org/10.1021/acs.chemmater.9b04092">https://www.doi.org/10.1021/acs.chemmater.9b04092</a>) as that document includes all changes made.

# Functional Nanoassemblies with Mirror-Image Chiroptical Properties Templated by a Single Homochiral DNA Strand

Shambhavi Tannir,<sup>a</sup> Lev Levintov,<sup>b</sup> Mark A. Townley,<sup>c</sup> Brian M. Leonard,<sup>a</sup> Jan Kubelka,<sup>d</sup> Harish Vashisth,<sup>b</sup> Krisztina Varga<sup>e\*</sup>, Milan Balaz<sup>f\*</sup>

- (a) University of Wyoming, Department of Chemistry, Laramie, WY 82071, USA.
- (b) University of New Hampshire, Department of Chemical Engineering, Durham, NH 03824, USA.
- (c) University of New Hampshire, University Instrumentation Center, Durham, NH 03824, USA.

- (d) University of Wyoming, Department of Petroleum Engineering, Laramie, WY 82071, USA.
- (e) University of New Hampshire, Department of Molecular, Cellular, and Biomedical Sciences, Durham, NH 03824, USA. E-mail: krisztina.varga@unh.edu
- (f) Yonsei University, Underwood International College, Integrated Science & Engineering Division, Seoul, 03722, Republic of Korea, E-mail: mbalaz@yonsei.ac.kr

ABSTRACT: For the supramolecular chemistry of self-assembly systems, a major goal is to achieve the level of control of the assembly process equal to the capabilities of classical asymmetric organic synthesis, such as high stereospecificity, regiospecificity, and reproducibility. Herein we report the stereoselective porphyrin-driven formation of left- and right-handed, chiral functional supramolecular nanoassemblies with mirror image chiroptical properties templated by a single homochiral ssDNA by changing the cooling rate, DMSO, and salt concentration. Upon dialysis and annealing that caused the porphyrin units to relax into their preferred slipped cofacial stacking geometry, the nanoassemblies displayed near ideal mirror-image chiroptical properties, as well as unusually high thermal and acid-base structural stability. ssDNA-porphyrin nanoassemblies preserved their photocatalytic activity in the visible spectral range as demonstrated by iodide oxidation. ssDNA-porphyrin nanoassemblies formed higher order fluorescent nano- and micro-structures as evidenced by TEM and confocal microscopy. We propose a plausible mechanism for the formation of nanoassemblies and induction of helicity based on our molecular dynamics (MD) simulations, time-dependent density functional theory

(TD DFT) computations and experimental spectroscopic data. We suggest that the ssDNA templates interact with preformed achiral porphyrin columnar nanostacks. These results provide further insight into the stereoselective synthesis of chiroptical nanostructures and control of supramolecular helicity.

Living organisms rely on assembly of molecules and biomolecules to prepare complex hierarchical systems with a wide range of structures and functionalities. Homochirality is a signature of biological systems, and it plays an integral part in biological self-assembly, biosynthesis, and molecular recognition. <sup>1-4</sup> The properties of supramolecular nanostructures highly depend on the degree of structural order, and an ultimate challenge of asymmetric supramolecular chemistry is to achieve the level of control of the assembly process that equals the capabilities of classical asymmetric organic synthesis (*i.e.*, high stereospecificity, regiospecificity, and reproducibility).

The assembly of achiral molecules along a chiral template is a common strategy to form chiral supramolecular polymers with electronic and chiroptical properties that are not present in individual molecules.<sup>5</sup> The final characteristics of the chiral assemblies, including their optical, chiroptical, and structural properties, are governed by the interplay between the template and the monomers (*e.g.*, hydrogen bonding,  $\pi$ – $\pi$  stacking, electrostatic, and van der Waals forces). Nucleic acids<sup>6-21</sup> and peptides<sup>22-31</sup> are commonly used as polymeric templates to prepare supramolecular multichromophoric nanoassemblies. As the example of right-handed B-DNA and left-handed Z-DNA illustrates, homochiral templates can yield supramolecular structures of opposite helicities (*i.e.*, conformational diastereomers). Pasternack and Purrello were the first to

explore single stranded DNA (ssDNA) as templates for chiral assembly utilizing electrostatic interactions between positively charged achiral chromophores and negative charged phosphate backbone. 32, 33 Schenning, Meijer, Shimizu, and coworkers pioneered the use of directional Hbonding for assembly of small organic molecules into helical supramolecular stacks on ssDNA templates. <sup>6, 10, 11, 27</sup> Despite considerable biological precedence, only two examples of structural polymorphism of homochiral ssDNA-templated nanoassemblies have been reported. 16 Schenning, Meijer and coworkers communicated that different helicities of ssDNA-templated diaminopurine-naphthalene conjugates can be obtained at different pH. 34 We have shown ssDNA-templated assembly of porphyrin-diaminopurine nanoassemblies with opposite but not mirror-image helical twists. 13, 14 In nature, porphyrinoids are components of many vital yet diverse structures such as light-harvesting complexes or hemoproteins. To develop further applications of porphyrin assemblies, the control of their specific arrangement into morphologically defined shapes is key. Achiral porphyrins are especially suitable building blocks for chiral functional nanoassemblies due to their strong affinity for self-stacking, their ability to control DNA structure and assembly, 35-37 and their (photo)chemical, electrochemical, and thermal stability. <sup>36, 38-40</sup> Moreover, artificial DNA-templated porphyrin assemblies have been used for light-harvesting, 41-44 sensing, 45-47 and gene delivery. 48

Herein we report on highly ordered left-handed and right-handed supramolecular porphyrin nanostructures templated between two strands of homochiral single stranded oligothymidylic acid ((**DZnPD**)<sub>40</sub>:(**T40**)<sub>2</sub>, Scheme 1) prepared under different experimental conditions (cooling rate, DMSO and NaCl concentrations) as evidenced by opposite but non-mirror-image CD spectra. Subsequent thermal annealing allowed the porphyrin units to relax into their preferred mirror-image stacking geometry yielding nanoassemblies with nearly perfect mirror-image

chiroptical properties. Molecular dynamics (MD) structural calculations with time-dependent density functional theory (TDDFT) simulations of CD spectra were used to propose assembly mechanism and assign the handedness of the nanoassemblies. Formation of higher order architectures was observed by transmission electron microscopy (TEM) and confocal laser scanning and polarized light microscopies (CLSM, PLM). Finally, porphyrin-DNA nanoassemblies retained their capacity to photocatalytically oxidize iodine. These findings will further contribute to the development of methods for assembly of chiral artificial supramolecular systems with multiple tunable structural and functional properties.

Scheme 1. T40 H-bond-templated assembly of zinc(II)-porphyrin diaminopurine conjugate **DZnPD** into chiral nanoassemblies.

### **Results and Discussion**

By screening different experimental assembly conditions, we found that the slow cooling, SC (0.25 °C/min; see ESI for detailed experimental procedure) of **DZnPD** (2 eq) with **T40** template (1 eq) from +85 °C to +20 °C in the presence of NaCl (200, 500, or 700 mM) yielded formation of chiral nano-assemblies of single preferred helicity, (referred to as SC), when the amount of DMSO was kept between 1% and 30% (Figure 1a and S1). No chiral assemblies were formed in the absence of NaCl. The most intense CD signal was obtained with 700 mM NaCl and 18% DMSO and displayed four CD bands in (+/-/+/-) pattern (from longer to shorter wavelength; Figure 1b, red curve). Using the exciton chirality method developed by Nakanishi, Harada, and Berova, <sup>49</sup> right-handed helicity (clockwise arrangement of **DZnPD** chromophores; P stereoisomer) was assigned to the SC assemblies based on the (+/-) bisignate CD signal in the Soret band region. On the other hand, fast cooling, FC (a non-linear temperature drop from 86 °C to 20 °C in ~3 min ( $\Delta T = -66$  °C); see ESI) of **DZnPD/T40** mixture in the absence of NaCl with DMSO concentration in the range 24-28% yielded left-handed nanoassemblies (M stereoisomer assigned by exciton chirality method). This assignment was subsequently verified by theoretical modeling of the assembly structure and CD spectra (see below). The strongest CD signal was detected for FC formed at 26% DMSO and displayed five CD bands with a (+/-/+/-/+) pattern (Figure 1b, blue curve). No FC chiral assemblies were observed (i) by fast cooling in the absence of NaCl at DMSO concentrations below 24% or above 28%, and (ii) under "switched" cooling conditions, i.e. slow cooling, in the absence of NaCl with DMSO concentration in the 24-28% range (Figure S2). FC and SC nanoassemblies displayed opposite but not mirror-image helicities (as evidenced by their opposite but non-mirror-image CD spectra, Figure 1b), as was expected for a pair of helical conformational diastereomers (similar to B/Z-DNA<sup>50</sup>) prepared with a template of a single chirality (*i.e.*, oligothymidylic acid, **T40**).

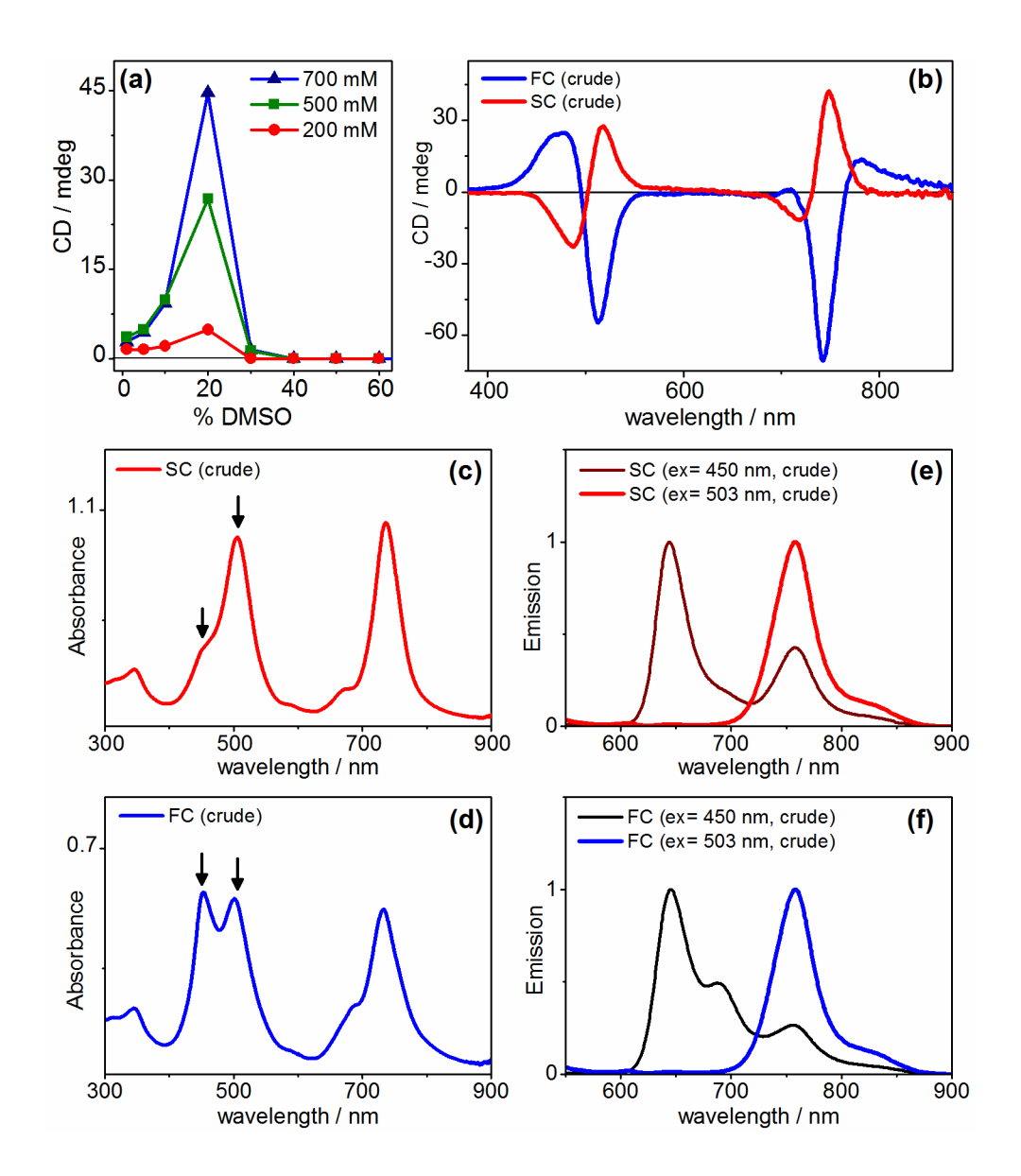


**Figure 1.** (a) Soret band CD signal of crude mixtures of **T40** templated **SC** porphyrin nanoassemblies (prepared by slow cooling) as a function of DMSO concentration for 700 mM, 500 mM and 200 mM NaCl. (b) CD spectra of crude mixtures of **T40** templated porphyrin nanoassemblies **FC** (blue curve; prepared by fast cooling) and **SC** (red curve; prepared by slow cooling). (c,d) UV-vis spectra (arrows denote excitation wavelengths) and (e,f) normalized

emission spectra ( $\lambda_{exc}$  = 450 or 503 nm) of crude **SC** and **FC** chiral nanoassemblies. Slow cooling: 0.5 °C/min with 1 min equilibration time after each 1 min step, 700 mM NaCl, 18% DMSO in 1.0 mM cacodylate buffer, pH = 7.0; fast cooling: 66 °C in ~3 min, 0 mM NaCl, 26% DMSO in 1.0 mM cacodylate buffer, pH = 7.0. [**SC\***] = [**FC\***] ~4  $\mu$ M

Importantly, fast- or slow-cooling of **DZnPD** with a non-complementary **dA40** template did not yield templated chiral nanoassemblies as evidenced by the absence of CD signal thus confirming the importance of H-bond directional recognition between the **DZnPD** chromophore and **T40** template in the formation of chiral assemblies (Figure S3).

UV-vis spectra of **SC** (Figure 1c) confirmed the formation of J-aggregates with very strong electronic coupling between **DZnPD** units as evidenced by a large red shift of the Soret band from 460.4 nm to 505.6 nm ( $\Delta$  = +45.2 nm) and of the Q band from 675.0 nm to 735.6 nm ( $\Delta$  = +60.6 nm). Similar strong red shifts of the Soret band to 502.0 nm ( $\Delta$  = +41.6 nm) and of the Q-band to 732.8 nm ( $\Delta$  = +57.8 nm) were observed for **FC** (Figure 1d). UV-vis absorption spectra showed lower assembly yield for **FC** than **SC** as evidenced by a presence of an absorption band at 453 nm in the **FC** sample (Figure 1d) corresponding to free **DZnPD** monomers, while only a small shoulder at 453 nm was observed in the **SC** sample (Figure 1c). Emission spectra were collected using two excitations wavelengths,  $\lambda_{\rm exc}$  =503 or 450 nm (Figure 1e,f). The former excited the newly formed **SC** and **FC** nanoassemblies and gave rise to single emission band centered around 758 nm whereas the latter preferentially excited the unassembled **DZnPD** monomers and yielded bands at 644 nm corresponding to the emission from the free **DZnPD**. Additional emission peak at 688 nm was observed for **FC** (Figure 1f) and probably originated

from misassembly (defective assembly) of a small number of porphyrin units as indicated by dialysis results (see below). The emission spectra provided additional confirmation of successful formation of nanoassemblies.

FC and SC nanoassemblies displayed opposite but not mirror-image CD spectra (Figure 1b). Without a chiral **T40** template, achiral **DZnPD** would form energetically favored slipped cofacial stacks of predetermined left-handed and right-handed mirror-image helicities in equal amounts therefore ultimately yielding racemic and CD inactive sample. The presence of chiral **T40** under appropriate experimental conditions allowed to break the symmetry and lead to controlled preferential formation of diastereomeric left-handed FC and right-handed SC nanoassemblies with opposite, non-mirror-image porphyrin-porphyrin cofacial stacking geometries. In order to obtain nanoassemblies with mirror-image CD spectra, we explored thermal annealing as a means to induce **DZnPD** to adopt its energetically favored cofacial stacking geometry in FC and SC nanoassemblies by overpowering the templating role of T40. We therefore dialyzed FC and SC nanoassemblies (2 kDa cassettes) to remove the DMSO, NaCl and the non-assembled or misassembled **DZnPD** (see ESI), <sup>13</sup> then thermally annealed them (heating at 85 °C for 20 min; see ESI) to yield FC\* and SC\* nanoassemblies (asterisk denotes dialyzed/annealed samples). While dialysis/annealing caused minimal changes in the SC sample (Figure 2b), it proved to be a quick yet efficient method to remove the majority of unassembled **DZnPD** from the FC sample as evidenced by disappearance of the 453 nm band and 685 nm shoulder in the UV-vis spectrum of the FC\* sample (Figure 2c). Dialysis alone already caused the disappearance of the emission peak at 688 nm (Figure S8). Comparisons of the CD spectra of the dialyzed/annealed FC\* and SC\* (Figure 2a) with the CD spectra of their crude FC and SC counterparts (Figure 1b) revealed that the CD signal phase changed in the Q-band region of FC\*.

Importantly, CD spectra of (P)-SC\* and (M)-FC\* displayed near perfect mirror-image CD profiles despite the assemblies being conformational diastereomers (**T40** ssDNA templates have the same (2R,4S,5R) central chirality of thymidine units in FC\* and SC\*). The mirror-image CD spectra are due to the strong energetically-favored slipped cofacial stacking between porphyrin units, together with the fact that the CD signature of the nanoassemblies in the visible region originates solely from the electronic coupling between asymmetrically oriented porphyrins, with no chiroptical contribution from the DNA template.  $^{51}$ 

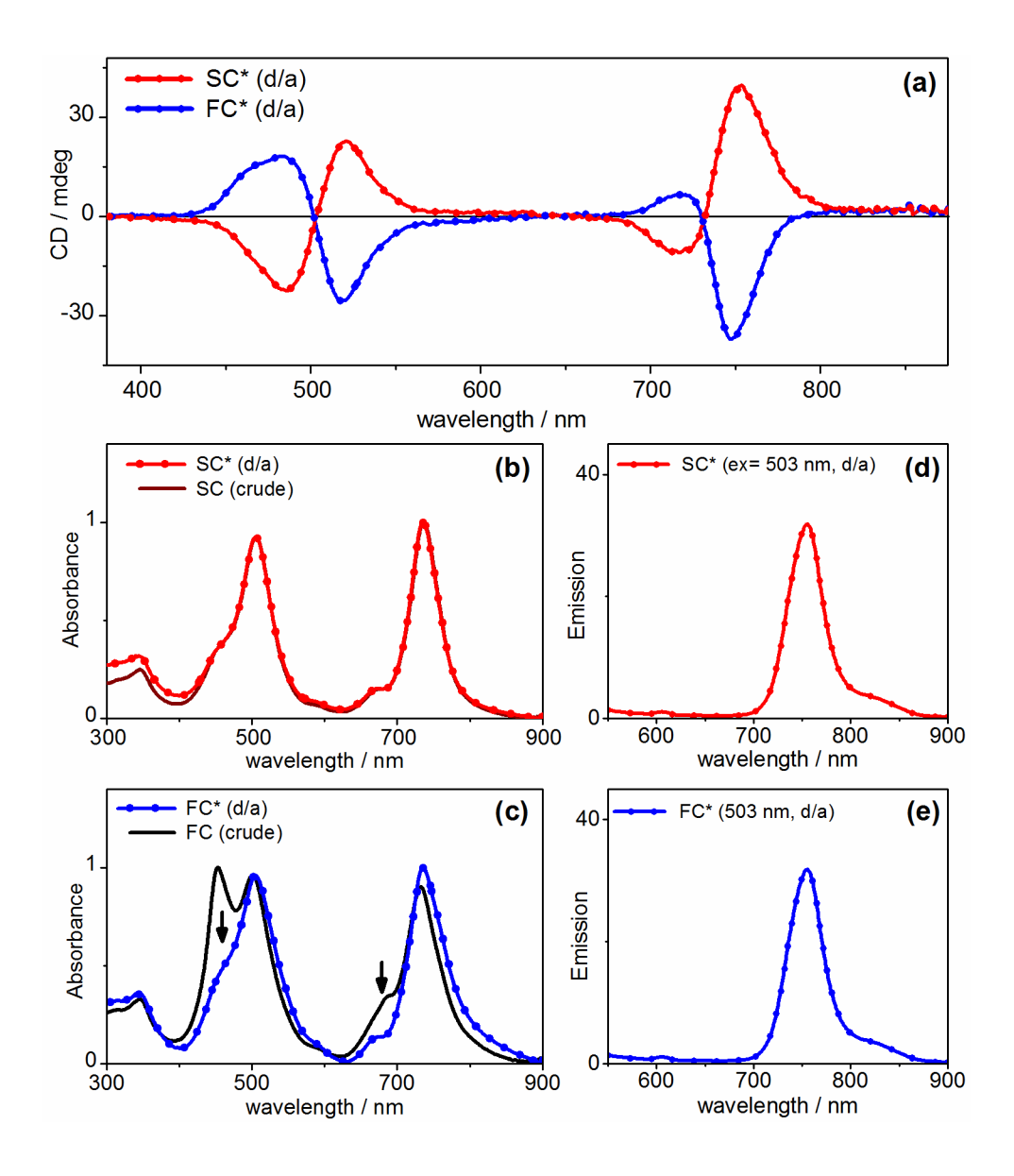


**Figure 2.** (a) CD spectra of dialyzed/annealed left-handed (*M*)-FC\* and right-handed (*P*)-SC\* chiral nanoassemblies. (b,c) Comparison of normalized UV-vis spectra of dialyzed/annealed SC\* and FC\* nanoassemblies (dashed lines) with crude SC and FC nanoassemblies (solid lines). Arrows highlight dialysis/annealing-induced removal of free **DZnPD** monomers. (d,e) Emission spectra ( $\lambda_{\text{exc}} = 503 \text{ nm}$ ) of dialyzed/annealed SC\* and FC\* chiral nanoassemblies.

Next we examined the thermal stability of crude (P)-SC and (M)-FC as well as dialyzed/annealed (P)-SC\* and (M)-FC\*. The variable temperature CD (vt-CD) of crude (M)-FC revealed melting above 40 °C and near complete disassembly at 85 °C (Figure 3a, blue curve), while no evidence of melting or racemization was observed for crude (P)-SC (Figure 3a, red curve). vt-CD of dialyzed and annealed (M)-FC\* and (P)-SC\* samples revealed very high thermal stability: no disassembly or racemization was observed when assemblies were heated for an extended period of time at +85 °C (Figure 3a, dotted solid curves) or allowed to stand in the dark at RT for several weeks (Figure S4). Chiroptical activity of (M)-FC\* and (P)-SC\* nanoassemblies in the visible region also displayed excellent pH resistance within the 6-12 and 2-12 pH range, respectively (Figures S5, S6), confirming strong intermolecular forces within porphyrin stacks. Altogether, the vt-CD data indicated that stereoselective interaction between the chiral **T40** template and **DZnPD** chromophores during assembly formation was under kinetic (FC) or thermodynamic (SC) control. Fast cooling (T-drop) conditions in the absence of NaCl appeared to favor formation of thermally labile left-handed conformational diastereomer (M)-FC (local energy minimum) with non-optimal porphyrin-porphyrin stacking geometry. On the other hand, the slow cooling conditions in the presence of NaCl favored the formation of thermally stable right-handed conformational diastereomer (P)-SC (global energy minimum) with optimal

porphyrin-porphyrin stacking geometry. Subsequent annealing converted the labile (M)-FC into thermally stable mirror-image (M)-FC\* (global energy minimum, Figure 3b) by allowing it to adopt optimal stacking geometry and stereochemically locked conformation.

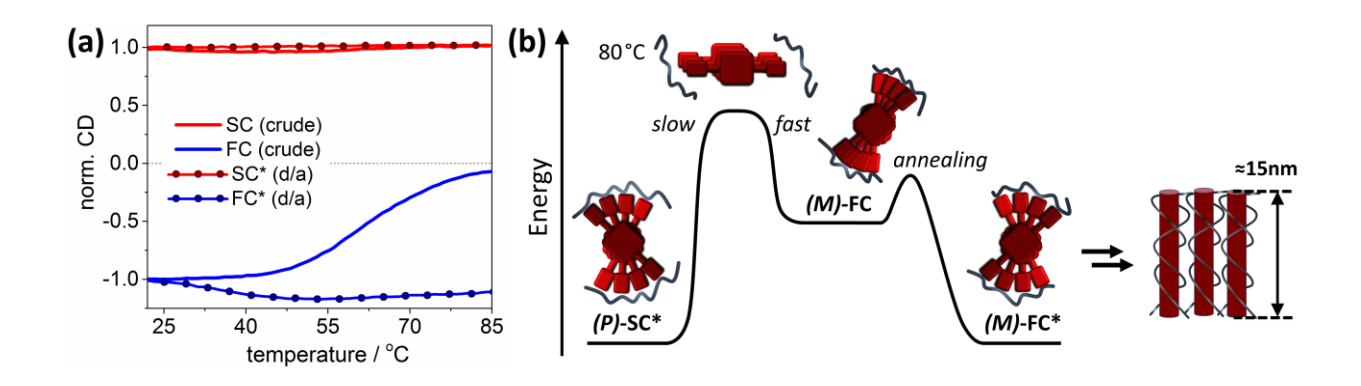


**Figure 3.** (a) Normalized vt-CD spectra of crude (P)-SC and (M)-FC and dialyzed/annealed (P)-SC\* and (M)-FC\* nanoassemblies (red curves,  $\lambda_{CD} = 530$  nm, blue curves,  $\lambda_{CD} = 511$  nm). Ramping rate: 5 °C/min. (b) Schematic energy diagram for the formation of DNA-templated porphyrin nanoassemblies under thermodynamic (SC) and kinetic (FC) control followed by higher order self-assembly to a stereochemically locked conformation.

The (M)-FC\* and (P)-SC\* nanoassemblies displayed exceptionally high values of opposite signs for specific rotations  $[\alpha]_D$  as well as for CD anisotropy g factors (also known as Kuhn's dissymmetry factors) for positive and negative Cotton effects in the Soret band and Q band regions (Table 1). Similar absolute values of  $[\alpha]_D$  as well as CD anisotropy of (P)-SC\* and (M)-FC\* suggested similar stereoselectivity of the assembly process by the homochiral ssDNA template. Although the experimental conditions allowed the stereoselectivity to be controlled and either of two helicities could be preferentially prepared, the optical purity of (P)-SC\* and (M)-FC\* nanoassemblies is unknown and could not be determined.

**Table 1.** Specific rotations and CD anisotropy factors, g, for (M)-FC\* and (P)-SC\* nanoassemblies.

	(P)-SC*	(M)-FC*
[α] <sub>D</sub>	+3,729° ± 185	-3,356° ± 187
g (+CD Soret band) <sup>a</sup>	2.2×10 <sup>-3</sup>	2.7×10 <sup>-3</sup>
g (-CD Soret band) <sup>b</sup>	2.4×10 <sup>-3</sup>	2.9×10 <sup>-3</sup>
g (+CD Q band) <sup>c</sup>	3.6×10 <sup>-3</sup>	2.2×10 <sup>-3</sup>
g (-CD Q band) <sup>d</sup>	1.3×10 <sup>-3</sup>	2.2×10 <sup>-3</sup>

<sup>&</sup>lt;sup>a</sup> Positive and <sup>b</sup> negative Cotton effect of the Soret band. <sup>c</sup> Positive and <sup>d</sup> negative Cotton effect of the Q band.

Molecular dynamics (MD) simulations were carried out to determine the probable mechanism of the assembly process. We hypothesized that the **DZnPD** molecules self-assembled into achiral columnar nanostacks in buffer/DMSO solution at 85 °C. Upon cooling, the DNA strands then recognized the columnar nanostacks, and a right- or left-handed twist of the **DZnPD** stacks was then induced depending on experimental conditions. Our hypothesis was based on the fact that the Soret band of **DZnPD** is red-shifted and broader when dissolved in a water/DMSO mixture at 85 °C (full width at half maximum, FWHM = 41.4 nm at 473.8 nm) than in neat methanol at RT (FWHM = 23.8 nm at 460.4 nm), suggesting that in the former a heterogeneous population of **DZnPD** nanostacks likely exists (Figure S7). Therefore, for the MD simulations, free base **DPD** molecules (MD simulations could not be performed on **DZnPD** as no appropriate forcefield was available for zinc porphyrin) were positioned on top of each other in an achiral stacked conformation and two antiparallel **T40** strands were added on the opposing sides of the (**DPD**)<sub>40</sub> stack (Figures 4a and S9a). The system was solvated using explicit water (TIP3P) molecules, and the overall charge of solvated systems was neutralized by Mg<sup>2+</sup> ions. No NaCl was added, thus

mimicking the experimental condition for the formation of left-handed FC nanoassemblies. After energy minimization (Figure S9b), the simulation was allowed to run for ~200 ns. The two T40 strands diffused through the aqueous environment towards the achiral (DPD)<sub>40</sub> stack as they interacted with it. At ~90 ns, counterclockwise twist of the (DPD)<sub>40</sub> stack started to appear as one T40 strand interacted with the whole (DPD)<sub>40</sub> stack, while the other interacted partially (Figure S9c). Detailed analysis showed that DPD molecules 9-24 of the (DPD)<sub>40</sub> (Figure 4a,b, black colored) interacted with both T40 strands and continued to rotate counterclockwise until a relatively stable left-handed helix was formed at ~140 ns and remained for the rest of the simulation (200 ns, Figures 4b and S9e). The MD simulation thus successfully reproduced the experimentally observed formation of left-handed nanoassemblies by fast cooling in the absence of NaCl. The analysis of the system over the last 60 ns revealed a center-to-center distance of two adjacent DPD of D<sub>1</sub> = 5.9 Å, the rise per DPD along the assembly's axis of D<sub>2</sub> = 3.6 Å, the rotation per DPD of -8.1°, and the length of the (DPD)<sub>40</sub> stack  $\approx$ 145 Å (Figure 4c).

Using these MD parameters, model **DPD** stacks were built (*e.g.*, trimer (**DPD**)<sub>3</sub>, Figure 4d) and their UV-vis and CD spectra and CD anisotropy *g* factors (Table S2) were simulated using TDDFT and/or simplified TDDFT (sTDDFT)<sup>52-54</sup> at B3LYP/6-31G(d) level (see Methods): trimer (**DPD**)<sub>3</sub> (Figure S10), hexamer (**DPD**)<sub>6</sub> (Figure S11 left), and decamer (**DPD**)<sub>10</sub> (Figures 4e and S11 right). The computed CD spectrum of (**DPD**)<sub>10</sub> (Figure 4e) had two bisignate (–/+) couplets and closely resembled the experimental data for the (*M*)-**FC**\* samples (Figure 1b, blue curve). The good agreement among the simulated CD spectra and calculated *g* factor for the left-handed (**DPD**)<sub>40</sub> geometry and experimental CD spectra of (*M*)-**FC** confirmed (i) the helicity of the latter to be left-handed, and (ii) the MD-calculated geometry of (**DPD**)<sub>40</sub>:(**T40**)<sub>2</sub> to be accurate.

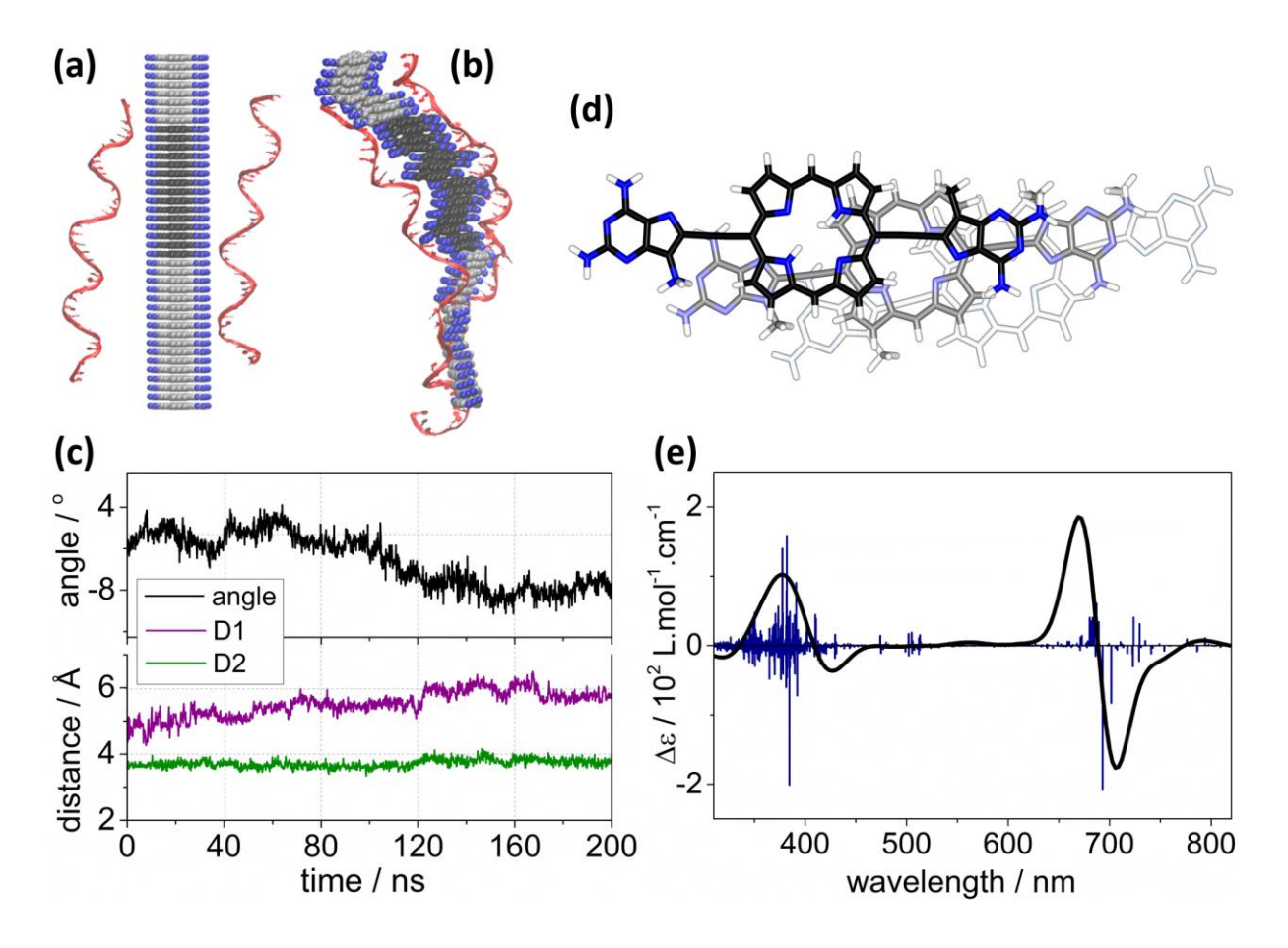
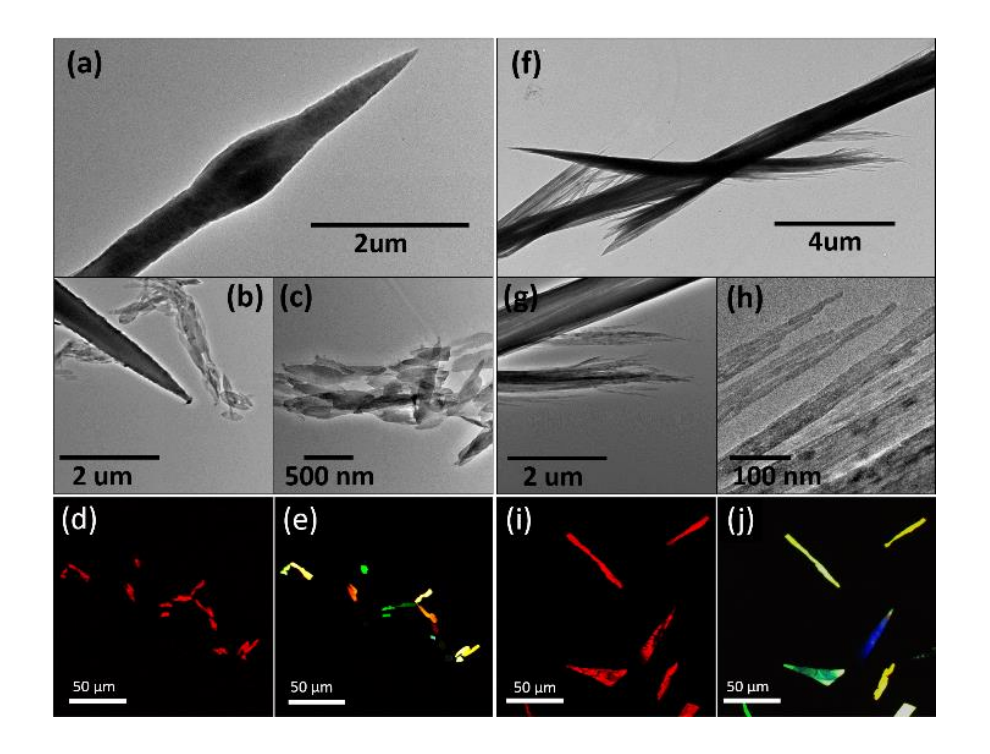


Figure 4. (a) Snapshots of the initial MD setup with two T40 strands and (DPD)<sub>40</sub> stack. (b) MD snapshot of the (DPD)<sub>40</sub>:(T40)<sub>2</sub> system at 200 ns. (c) MD trajectories of rotation per DPD (angle), center-to-center distance of two adjacent DPD (D1), and the rise per DPD along the assembly's axis (D2). (d) Model (DPD)<sub>3</sub> stack with MD calculated geometry (angle = 8.1°). (e) Simulated CD spectrum for model (DPD)<sub>10</sub> assembly. The spectra were calculated at B3LYP/6-31G(d) level using sTDDFT methodology with 7 eV (177 nm) cutoff. Spectral intensities are normalized per DPD unit. The vertical bars represent individual transitions; the spectra contours were simulated by assigning Gaussian band shapes with FWHM of 40 cm<sup>-1</sup> to each transition.

TEM imaging of the  $(\mathbf{DZnPD})_{40}$ : $(\mathbf{T40})_2$  nanoassemblies revealed that both (M)-FC\* and (P)-SC\* samples form similar, several microns long wires that vary in width from 100 nm to

microns. However, high-resolution images showed that although both samples have common ~20 nm features likely originating from the ordered side by side assembly of the individual DNA-porphyrin nanoassemblies (see Figure 3b), they formed fairly different higher order nanostructures likely depending on the stacking and offset of the nanoassemblies. The (M)-FC\* sample was composed of smaller scale-like structures that appeared to form into the larger micron-size wires with very sharp points at their ends (Figure 5a) but were always present as individual scales (Figures 5b,c). These scales were 150 nm in width and 500 nm in length. The height of these scales was difficult to determine but was approximately 20 nm based on the few vertically aligned scales observed (e.g., Figure 5c) and the light contrast compared to other objects. On the other hand, the (P)-SC\* sample was made of small wires roughly 20 nm in diameter that clumped together into a hierarchical structure ultimately resulting in large micronsize wires that were frayed apart near the end. Figure 5f highlights the fraying of the microwires into nanowires, and Figures 5g,h show the individual ~20 nm wide nanowires. Polarized light microscopy (PLM, Figures 5e, j; see ESI for detailed experimental procedure) and confocal laser scanning microscopy (CLSM, Figures 5d,i) revealed that the (M)-FC\* and (P)-SC\* nanoassemblies formed micron-sized anisotropic crystals that fluoresced strongly in the red (703-799 nm) when excited by green light (514 nm).



**Figure 5.** (a-c) Bright field TEM, (d) CLSM, and (e) PLM images of dialyzed/annealed (M)-**FC\*** nanoassemblies. (f-h) Bright field TEM, (i) CLSM, and (j) PLM images of dialyzed/annealed (P)-**SC\*** nanoassemblies. For CLSM images (d) and (i),  $\lambda_{Ex} = 514$  nm,  $\lambda_{Em} = 703-799$  nm.

One of the principal objectives in the synthesis of supramolecular nanomaterials is incorporation of sustainable functional properties. We have therefore explored the photocatalytic formation of triiodide from iodide in the presence of **SC\*** and **FC\*** nanoassemblies. Iodide oxidation was previously been used to assess the photocatalytic activity of peptide-templated porphyrin nanoassemblies.<sup>28, 30</sup> The light-induced oxidation of iodide to triiodide (see ESI) was successfully induced by 532 nm light irradiation of nanoassemblies (*P*)-**SC\*** or (*M*)-**FC\***, as proven by an increase in 350 nm band intensity in the time dependent UV-vis absorption spectra associated with I<sub>3</sub><sup>-</sup> anion generation (Figure 6b, blue circles and red squares). Photocatalytic activity of **DZnPD** has therefore been preserved in the assemblies. **DZnPD** aggregates prepared

in the absence of **T40** template exhibited similar photocatalytic activity (Figure 6b, green triangles), while a control experiment in the absence of **DZnPD** showed no changes in the intensity of the 350 nm absorption peak after exposure to light (Figure 6b, black diamonds), confirming that the nanoassemblies acted as photosynthetic systems.

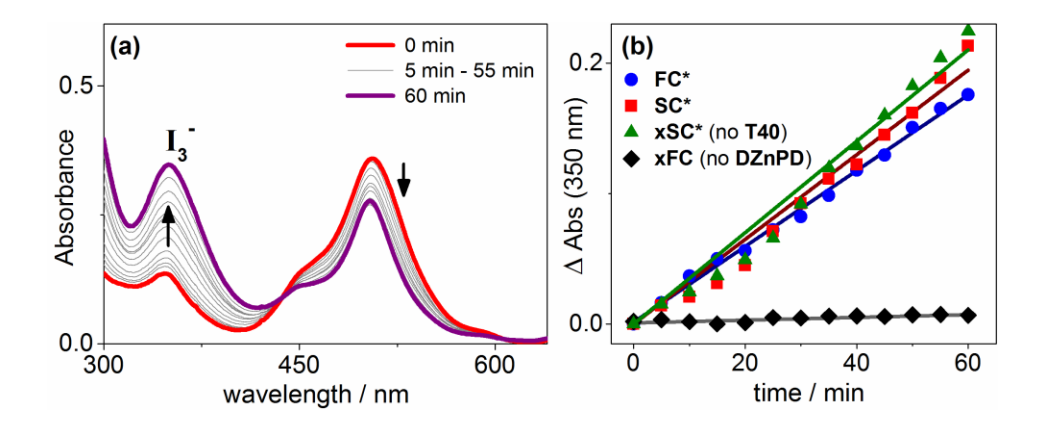


**Figure 6.** (a) Time dependent UV-vis absorption spectra quantifying the photocatalytic synthesis of triiodide by (*P*)-SC\* assembly ( $\lambda_{irr}$  = 532 nm, 5 mW, [NaI] = 500 mM, [SC\*] ~4 μM), showing formation of I<sub>3</sub><sup>-</sup> *via* an increase of the 350 nm peak intensity. (b) Plots of absorption intensity ( $\lambda$  = 350 nm; I<sub>3</sub><sup>-</sup>) against the irradiation time for triiodide production catalyzed by (*P*)-SC\* (red squares) and (*M*)-FC\* (blue circles) nanoassemblies and their linear fits. Control experiments: FC without **DZnPD** (diamond squares) and SC\* without **T40** (green triangles) and their linear fits.

### **Conclusion**

We have shown that highly ordered chiral, optically active supramolecular porphyrin nanoassemblies can be templated between two strands of non-self-complementary homochiral ssDNA template, and their handedness can be controlled using experimental conditions. Kinetic and thermodynamic conditions have been successfully used to obtain either left-handed (*M*)-FC

or right-handed (P)-SC nanoassemblies, respectively. Their dialysis and thermal annealing yielded (M)-FC\* and (P)-SC\* with near ideal mirror-image CD and specific rotation characteristics due to the porphyrins' high propensity for self-stacking, which controlled the final geometry as well as chiroptical properties. (M)-FC\* and (P)-SC\* nanoassemblies displayed unusually high thermal and acid-base structural robustness and no racemization or disassembly has been observed. Based on experimental spectroscopic evidence, we proposed a plausible mechanism for the formation of the nanoassemblies and helicity induction using molecular dynamic simulations and time-dependent density functional theory computations. ssDNA templates interacted with initially formed achiral porphyrin nanostacks via H-bond complementarity, and depending on the experimental conditions, yielded preferably right-handed or left-handed helical twist. (M)-FC\* and (P)-SC\* nanoassemblies exhibited photocatalytic activity in the visible spectral range through iodide oxidation. (M)-FC\* and (P)-SC\* nanoassemblies formed higher order nano- and micro-structures of different morphologies with (P)-SC\* assembling into nanowires and (M)-FC\* assembling into nanoscales. Crystals formed from either of the two nanoassemblies, on the order of microns in size, were birefringent and fluoresced red upon green light excitation. The assemblies displayed photocatalytic activity as evidenced by photooxidation of iodide to triiodide. These findings will further contribute to the development of methods for stereoselective assembly of robust chiral supramolecular systems with tunable structural and functional properties. Chiral materials could find applications in stereoselective catalysis, in chirality-dependent photoluminescent materials or as chiral bridges for room-temperature photospintronics.

## Methods

System setup and simulations: All molecular dynamics (MD) simulations were carried out and analyzed using the NAMD/VMD software suite. 55, 56 The AMBER bsc1 force field 57 was used to simulate DNA strands. The initial structure of an oligothymidylic acid T40 was created using the psfgen tool in VMD by using the topology information of a single thymine nucleotide. To prepare the initial system, coordinates, charges, and the AMBER force field parameters of the porphyrin-diaminopurine (**DPD**) molecule were developed. At first, the initial structure of the **DPD** molecule was created using CHARMM-GUI *Ligand-Reader and Modeler*<sup>58, 59</sup> followed by 100 steps of conjugate gradient energy minimization in NAMD. Then, the "antechamber" program<sup>60, 61</sup> in AMBER was used to obtain force field parameters and the AM1-BCC charge method<sup>62</sup> was used to obtain atomic charges. After developing parameters, 40 **DPD** molecules were positioned on top of each other in an achiral stacked conformation and two T40 strands were added on the opposite sides of the stack. All systems were solvated using explicit water (TIP3P) molecules and the overall charge of solvated systems was neutralized by adding Mg<sup>2+</sup> ions. Detailed information on system-size and trajectory length is provided in Table S1. The box volume was optimized in the NPT ensemble by first running a 1000 step conjugate gradient energy minimization that was followed by a 400 ps MD run with a 2 fs time step. The temperature in all simulations was maintained at 310 K and controlled using the Langevin thermostat and the pressure was controlled by the Nose-Hoover barostat in all NPT runs. All simulations were carried out using periodic boundary conditions. The simulations were further run in the NVT ensemble after brief initial equilibration in the NPT ensemble. Long-range electrostatic interactions were treated by the particle-mesh Ewald method.<sup>63</sup> Computations were performed on Premise, an in-house GPU based cluster, and on supercomputing resources of the Extreme Science and Engineering Discovery Environment (XSEDE).<sup>64</sup>

Quantum mechanical simulations of the UV-VIS and CD spectra: All quantum mechanical calculations were done with Gaussian 09 package.  $^{65}$  Model structures were built from a  $C_{2h}$ porphyrin **DPD** (Scheme 1) monomer whose geometry was optimized at B3LYP/6-31G(d) level. Stacks of 3 (trimer), 6 (hexamer), and 10 (decamer) **DPD** units were assembled from the optimized monomers with distances and angles obtained from the MD simulations of the (**DPD**)<sub>40</sub>:(**T40**)<sub>2</sub> assemblies. UV-vis and CD spectra simulations were carried out using the sTDDFT method<sup>52-54</sup> with B3LYP/6-31G(d) level ground state DFT calculations and an energy cutoff of 7 eV (177 nm). Absorption intensities were calculated using the length formalism, while CD with the velocity formalism. 52 As a benchmark, a full TDDFT B3LYP/6-31G(d) excited state calculation was also performed for the trimer (DPD)3. The dipole and rotational strengths for the calculations of UV-vis absorption and CD spectra were computed, respectively, using the length and velocity formalisms. Spectral contours were simulated by assigning Gaussian bandshapes with 40 nm width (FWHM – Full Width at Half Maximum) to all transitions. The intensities were normalized per unit **DPD** (i.e., effectively per mole of **DPD**) to highlight the effect of the assembly size on the CD signals. Further tests of the reliability of the calculations were performed by including an implicit solvent (polarized continuum)<sup>65</sup> model for water, basis set effects using a smaller 3-21G set, and a range-separated DFT (CAM-B3LYP). Both solvent and basis set had relatively minor effects as seen previously, <sup>13</sup> while CAM-B3LYP, which often helps eliminate spurious low-lying CT states, <sup>66</sup> gave significantly blue-shifted spectra (data not shown).

# **Supporting Information**

Materials, methods and instrumentation, synthesis of **DZnPD**. Experimental conditions for DNA-templated assembly of **FC** and **SC**, dialysis, thermal annealing, and photo-oxidation. CD

spectra for pH and time stability, UV-vis spectra of **DZnPD**, molecular dynamics calculations, TDDFT calculations.

## Acknowledgment

This work was supported in part by the National Science Foundation (award CBET-1403947; KV, JK; CBET-1554558; HV). MB thanks Yonsei University and KV thanks the University of New Hampshire for the support. We acknowledge computational support through the following resources: Premise, a central shared HPC cluster at UNH supported by the Research Computing Center; BioMade, a heterogeneous CPU/GPU cluster supported by the NSF EPSCoR award (OIA-1757371; HV); and the NSF-supported (ACI-1548562) Extreme Science and Engineering Discovery Environment (XSEDE) Comet resource at San Diego Supercomputer Center (SDSC) under grant TG-MCB160183 (HV). We thank G. Sargsyan (UW) for his assistance with the synthesis of porphyrins and J. Laird (University of New Hampshire) for the use of the polarized light microscope.

### **Abbreviations**

FC, nanoassembly prepared by fast-cooling; SC, nanoassembly prepared by slow-cooling; SC\*, dialyzed and annealed slow-cooled nanoassembly; FC\*, dialyzed and annealed fast-cooled nanoassembly; **T40**, oligothymidylic acid; **DPD**, diaminopurine porphyrin; **DZnPD**, diaminopurine zinc(II)porphyrin; CD, circular dichroism; *vt*-CD, variable temperature CD; TEM, transmission electron microscopy; DFT, density functional theory; TDDFT, time dependent DFT; CLSM, confocal laser scanning microscopy; PLM, polarized light microscopy; MD, molecular dynamics; FWHM, full width at half maximum.

# **Corresponding Authors**

Dr. Milan Balaz mbalaz@yonsei.ac.kr, Dr. Krisztina Varga krisztina.varga@unh.edu

### **Additional Information**

Competing interests: authors declare no competing financial interests.

# **REFERENCES**

- 1. Salam, A. The Role of Chirality in the Origin of Life. J. Mol. Evol. 1991, 33, 105-113.
- 2. Pavlov, V. A.; Klabunovskii, E. I. Homochirality Origin in Nature: Possible Versions. *Curr. Org. Chem.* **2014**, *18*, 93-114.
- 3. Crusats, J.; Veintemillas-Verdaguer, S.; Ribo, J. M. Homochirality as a Consequence of Thermodynamic Equilibrium? *Chem. Eur. J.* **2006**, *12*, 7776-7781.
- 4. Buschmann, H.; Thede, R.; Heller, D. New Developments in the Origins of the Homochirality of Biologically Relevant Molecules. *Angew. Chem. Int. Ed.* **2000**, *39*, 4033-4036.
- 5. Aida, T.; Meijer, E. W.; Stupp, S. I. Functional Supramolecular Polymers. Science 2012, 335, 813-817.
- 6. Iwaura, R.; Hoeben, F. J. M.; Masuda, M.; Schenning, A.; Meijer, E. W.; Shimizu, T. Molecular-Level Helical Stack of a Nucleotide-Appended Oligo(*p*-Phenylenevinylene) Directed by Supramolecular Self-Assembly with a Complementary Oligonucleotide as a Template. *J. Am. Chem. Soc.* **2006**, *128*, 13298-13304.
- 7. Nakamura, M.; Okaue, T.; Takada, T.; Yamana, K. DNA-Templated Assembly of Naphthalenediimide Arrays. *Chem. Eur. J.* **2012**, *18*, 196-201.
- 8. Xiao, J.; Li, J.; Li, C.; Huang, C.; Li, Y.; Cui, S.; Wang, S.; Liu, H. Mg<sup>2+</sup>-Mediated Self-Assembly of an Amphiphilic Pyrene Derivative with Single-Stranded DNA. *Tetrahedron Lett.* **2008**, *49*, 2656-2660.
- 9. Paolantoni, D.; Rubio-Magnieto, J.; Cantel, S.; Martinez, J.; Dumy, P.; Surin, M.; Ulrich, S. Probing the Importance of π-Stacking Interactions in DNA-Templated Self-Assembly of Bisfunctionalized Guanidinium Compounds. *Chem. Commun.* **2014**, *50*, 14257-14260.
- 10. Janssen, P. G. A.; Vandenbergh, J.; van Dongen, J. L. J.; Meijer, E. W.; Schenning, A. Ssdna Templated Self-Assembly of Chromophores. *J. Am. Chem. Soc.* **2007**, *129*, 6078-6079.
- 11. Janssen, P. G. A.; Jabbari-Farouji, S.; Surin, M.; Vila, X.; Gielen, J. C.; de Greef, T. F. A.; Vos, M. R. J.; Bomans, P. H. H.; Sommerdijk, N.; Christianen, P. C. M.; Leclere, P.; Lazzaroni, R.; van der Schoot, P.; Meijer, E. W.; Schenning, A. Insights into Templated Supramolecular Polymerization: Binding of Naphthalene Derivatives to Ssdna Templates of Different Lengths. *J. Am. Chem. Soc.* **2009**, *131*, 1222-1231.
- 12. Zhang, N.; Chu, X. Z.; Fathalla, M.; Jayawickramarajah, J. Photonic DNA-Chromophore Nanowire Networks: Harnessing Multiple Supramolecular Assembly Modes. *Langmuir* **2013**, *29*, 10796-10806.
- 13. Sargsyan, G.; Leonard, B. M.; Kubelka, J.; Balaz, M. Supramolecular ssDNA Templated Porphyrin and Metalloporphyrin Nanoassemblies with Tunable Helicity. *Chem. Eur. J.* **2014**, *20*, 1878-1892.
- 14. Sargsyan, G.; Schatz, A. A.; Kubelka, J.; Balaz, M. Formation and Helicity Control of ssDNA Templated Porphyrin Nanoassemblies. *Chem. Commun.* **2013**, *49*, 1020-1022.
- 15. Stulz, E. Nanoarchitectonics with Porphyrin Functionalized DNA. Acc. Chem. Res. 2017, 50, 823-831.
- 16. Balaz, M.; Tannir, S.; Varga, K. Chiral Multichromophoric Supramolecular Nanostructures Assembled by Single Stranded DNA and RNA Templates. *Coord. Chem. Rev.* **2017**, *349*, 66-83.
- 17. Hofsäβ, R.; Ensslen, P.; Wagenknecht, H.-A. Control of Helical Chirality in Supramolecular Chromophore–DNA Architectures. *Chem. Commun.* **2019**, *55*, 1330-1333.

- 18. Rubio-Magnieto, J.; Phan, T. A.; Fossepre, M.; Matot, V.; Knoops, J.; Jarrosson, T.; Dumy, P.; Serein-Spirau, F.; Niebel, C.; Ulrich, S.; Surin, M. Photomodulation of DNA-Templated Supramolecular Assemblies. *Chem. Eur. J.* **2018**, *24*, 706-714.
- 19. D'Urso, A.; Mammana, A.; Balaz, M.; Holmes, A. E.; Berova, N.; Lauceri, R.; Purrello, R. Interactions of a Tetraanionic Porphyrin with DNA: From a Z-DNA Sensor to a Versatile Supramolecular Device. *J. Am. Chem. Soc.* **2009**, *131*, 2046-2047.
- 20. Pasternack, R. F.; Gibbs, E. J. Porphyrin Interactions with Nucleic-Acids. *Inorganica Chimica Acta-Bioinorganic Chemistry* **1983**, *79*, 7-7.
- 21. Gibbs, E. J.; Tinoco, I.; Maestre, M. F.; Ellinas, P. A.; Pasternack, R. F. Self-Assembly of Porphyrins on Nucleic-Acid Templates. *Biochem. Biophys. Res. Commun.* **1988**, *157*, 350-358.
- 22. Purrello, R.; Scolaro, L. M.; Bellacchio, E.; Gurrieri, S.; Romeo, A. Chiral H- and J-Type Aggregates of Meso-Tetrakis(4-Sulfonatophenyl)Porphine on Alpha-Helical Polyglutamic Acid Induced by Cationic Porphyrins. *Inorg. Chem.* **1998**, *37*, 3647-3648.
- 23. Purrello, R.; Bellacchio, E.; Gurrieri, S.; Lauceri, R.; Raudino, A.; Scolaro, L. M.; Santoro, A. M. pH Modulation of Porphyrins Self-Assembly onto Polylysine. *J. Phys. Chem. B* **1998**, *102*, 8852-8857.
- 24. Gurrieri, S.; Aliffi, A.; Bellacchio, E.; Lauceri, R.; Purrello, R. Spectroscopic Characterization of Porphyrin Supramolecular Aggregates on Poly-Lysine and Their Application to Quantitative DNA Determination. *Inorg. Chim. Acta* **1999**, *286*, 121-126.
- Sakamoto, M.; Ueno, A.; Mihara, H. Construction of Alpha-Helical Peptide Dendrimers Conjugated with Multi-Metalloporphyrins: Photoinduced Electron Transfer on Dendrimer Architecture. *Chem. Commun.* 2000, 1741-1742.
- 26. Matsui, H.; MacCuspie, R. Metalloporphyrin Nanotube Fabrication Using Peptide Nanotubes as Templates. *Nano Lett.* **2001**, *1*, 671-675.
- 27. Lin, J.; Surin, M.; Beljonne, D.; Lou, X.; van Dongen, J. L. J.; Schenning, A. P. H. J. On the Mechanism of Dynamic Polymerization Via Recycled ss-DNA Templated Assembly of Non-Natural Bases. *Chem. Sci.* **2012**, *3*, 2732-2736.
- 28. Zou, Q. L.; Zhang, L.; Yan, X. H.; Wang, A. H.; Ma, G. H.; Li, J. B.; Mohwald, H.; Mann, S. Multifunctional Porous Microspheres Based on Peptide-Porphyrin Hierarchical co-Assembly. *Angew. Chem. Int. Ed.* **2014**, *53*, 2366-2370.
- 29. Kim, J. H.; Nam, D. H.; Lee, Y. W.; Nam, Y. S.; Park, C. B. Self-Assembly of Metalloporphyrins into Light-Harvesting Peptide Nanofiber Hydrogels for Solar Water Oxidation. *Small* **2014**, *10*, 1272-1277.
- 30. Liu, K.; Xing, R. R.; Chen, C. J.; Shen, G. Z.; Yan, L. Y.; Zou, Q. L.; Ma, G. H.; Mohwald, H.; Yan, X. H. Peptide-Induced Hierarchical Long-Range Order and Photocatalytic Activity of Porphyrin Assemblies. *Angew. Chem. Int. Ed.* **2015**, *54*, 500-505.
- 31. Koti, A. S. R.; Periasamy, N. Self-Assembly of Template-Directed J-Aggregates of Porphyrin. *Chem. Mater.* **2003**. *15*, 369-371.
- 32. Bustamante, C.; Gurrieri, S.; Pasternack, R. F.; Purrello, R.; Rizzarelli, E. Interaction of Water-Soluble Porphyrins with Single- and Double-Stranded Polyribonucleotides. *Biopolymers* **1994**, *34*, 1099-1104.
- 33. Pasternack, R. F.; Gurrieri, S.; Lauceri, R.; Purrello, R. Single-Stranded Nucleic Acids as Templates for Porphyrin Assembly Formation. *Inorg. Chim. Acta* **1996**, *246*, 7-12.
- 34. Janssen, P. G. A.; Ruiz-Carretero, A.; González-Rodríguez, D.; Meijer, E. W.; Schenning, A. P. H. J. Ph-Switchable Helicity of DNA-Templated Assemblies. *Angew. Chem. Int. Ed.* **2009**, *48*, 8103-8106.
- 35. Balaz, M.; Li, B. C.; Ellestad, G. A.; Berova, N. Tetraarylporphyrin as a Selective Molecular Cap for the Non Watson-Crick Guanine-Adenine Base Pair Sequences. *Angew. Chem. Int. Ed.* **2006**, *45*, 3530-3533.
- 36. Sargsyan, G.; Balaz, M. Porphyrin-DNA Conjugates: Porphyrin Induced Adenine-Guanine Homoduplex Stabilization and Interduplex Assemblies. *Org. Biomol. Chem.* **2012**, *10*, 5533-5540.
- 37. Fendt, L. A.; Bouamaied, I.; Thoni, S.; Amiot, N.; Stulz, E. DNA as Supramolecular Scaffold for Porphyrin Arrays on the Nanorneter Scale. *J. Am. Chem. Soc.* **2007**, *129*, 15319-15329.
- 38. Jurow, M.; Schuckman, A. E.; Batteas, J. D.; Drain, C. M. Porphyrins as Molecular Electronic Components of Functional Devices. *Coord. Chem. Rev.* **2010**, *254*, 2297-2310.
- Lauceri, R.; Fasciglione, G. F.; D'Urso, A.; Marini, S.; Purrello, R.; Coletta, M. Kinetic Investigation of Porphyrin Interaction with Chiral Templates Reveals Unexpected Features of the Induction and Self-Propagation Mechanism of Chiral Memory. *J. Am. Chem. Soc.* 2008, 130, 10476-10477.
- 40. Bottari, G.; Trukhina, O.; Ince, M.; Torres, T. Towards Artificial Photosynthesis: Supramolecular, Donor-Acceptor, Porphyrin-and Phthalocyanine/Carbon Nanostructure Ensembles. *Coord. Chem. Rev.* **2012**, *256*, 2453-2477.

- 41. Bae, A. H.; Hatano, T.; Sugiyasu, K.; Kishida, T.; Takeuchia, M.; Shinkai, S. Supramolecular Design of a Porphyrin-[60]Fullerene Photocurrent Generation System on a DNA Scaffold Fabricated by a Conjugate Polymer Film. *Tetrahedron Lett.* **2005**, *46*, 3169-3173.
- 42. D'Souza, F.; Das, S. K.; Zandler, M. E.; Sandanayaka, A. S. D.; Ito, O. Bionano Donor-Acceptor Hybrids of Porphyrin, ssDNA, and Semiconductive Single-Wall Carbon Nanotubes for Electron Transfer Via Porphyrin Excitation. *J. Am. Chem. Soc.* **2011**, *133*, 19922-19930.
- 43. Zhang, H. Y.; Bork, M. A.; Riedy, K. J.; McMillin, D. R.; Choi, J. H. Understanding Photophysical Interactions of Semiconducting Carbon Nanotubes with Porphyrin Chromophores. *J. Phys. Chem. C* **2014**, *118*, 11612-11619.
- 44. Zhang, H. Y.; Baker, B. A.; Cha, T. G.; Sauffer, M. D.; Wu, Y. J.; Hinkson, N.; Bork, M. A.; McShane, C. M.; Choi, K. S.; McMillin, D. R.; Choi, J. H. DNA Oligonucleotide Templated Nanohybrids Using Electronic Type Sorted Carbon Nanotubes for Light Harvesting. *Adv. Mater.* **2012**, *24*, 5447-5451.
- 45. Lei, J. P.; Ju, H. X.; Ikeda, O. Supramolecular Assembly of Porphyrin Bound DNA and Its Catalytic Behavior for Nitric Oxide Reduction. *Electrochim. Acta* **2004**, *49*, 2453-2460.
- 46. Liu, G. P.; Wu, Y. M.; Yuan, Y. L.; Chai, Y. Q.; Wei, S. Q.; Zhang, D. J. Manganese(III)Meso-Tetrakis(4-N-Methylpyridyl)-Porphyrin and Mediator Thionine co-Decorated DNA Nanowires for Sensitive Electrochemical Monitoring of Mercury(II). *RSC Adv.* **2014**, *4*, 52117-52122.
- 47. Zang, Y.; Lei, J. P.; Ling, P. H.; Ju, H. X. Catalytic Hairpin Assembly-Programmed Porphyrin-DNA Complex as Photoelectrochemical Initiator for DNA Biosensing. *Anal. Chem.* **2015**, *87*, 5430-5436.
- 48. Nishiyama, N.; Iriyama, A.; Jang, W. D.; Miyata, K.; Itaka, K.; Inoue, Y.; Takahashi, H.; Yanagi, Y.; Tamaki, Y.; Koyama, H.; Kataoka, K. Light-Induced Gene Transfer from Packaged DNA Enveloped in a Dendrimeric Photosensitizer. *Nat. Mater.* **2005**, *4*, 934-941.
- 49. Harada, N.; Nakanishi, K.; Berova, N. In *Comprehensive Chiroptical Spectroscopy*; Berova, N., Polavarapu, P. L., Nakanishi, K., Woody, R. W., Eds.; John Wiley & Sons, Inc.: Hoboken, NJ, 2012; Chapter 4, pp 115-166.
- 50. Choi, J. K.; Reed, A.; Balaz, M. Chiroptical Properties, Binding Affinity, and Photostability of a Conjugated Zinc Porphyrin Dimer Complexed with Left-Handed Z-DNA and Right-Handed B-DNA. *Dalton Trans.* **2014**, 43, 563-567.
- 51. Mammana, A.; Pescitelli, G.; Asakawa, T.; Jockusch, S.; Petrovic, A. G.; Monaco, R. R.; Purrello, R.; Turro, N. J.; Nakanishi, K.; Ellestad, G. A.; Balaz, M.; Berova, N. Role of Environmental Factors on the Structure and Spectroscopic Response of 5'-DNA-Porphyrin Conjugates Caused by Changes in the Porphyrin-Porphyrin Interactions. *Chem. Eur. J.* **2009**, *15*, 11853-11866.
- 52. Bannwarth, C.; Grimme, S. A Simplified Time-Dependent Density Functional Theory Approach for Electronic Ultraviolet and Circular Dichroism Spectra of Very Large Molecules. *Comp. Theor. Chem.* **2014**, *1040–1041*, 45-53.
- 53. Grimme, S. A Simplified Tamm-Dancoff Density Functional Approach for the Electronic Excitation Spectra of Very Large Molecules. *J. Chem. Phys.* **2013**, *138*, 244104.
- 54. Grimme, S.; Bannwarth, C. Ultra-Fast Computation of Electronic Spectra for Large Systems by Tight-Binding Based Simplified Tamm-Dancoff Approximation (Stda-Xtb). *J. Chem. Phys.* **2016**, *145*, 054103.
- 55. C., P. J.; Rosemary, B.; Wei, W.; James, G.; Emad, T.; Elizabeth, V.; Christophe, C.; D., S. R.; Laxmikant, K.; Klaus, S. Scalable Molecular Dynamics with Namd. *J. Comput. Chem.* **2005**, *26*, 1781-1802.
- 56. Humphrey, W.; Dalke, A.; Schulten, K. Vmd: Visual Molecular Dynamics. *Journal of Molecular Graphics* **1996**, *14*, 33-38.
- 57. Ivani, I.; Dans, P. D.; Noy, A.; Pérez, A.; Faustino, I.; Hospital, A.; Walther, J.; Andrio, P.; Goñi, R.; Balaceanu, A.; Portella, G.; Battistini, F.; Gelpí, J. L.; González, C.; Vendruscolo, M.; Laughton, C. A.; Harris, S. A.; Case, D. A.; Orozco, M. Parmbsc1: A Refined Force Field for DNA Simulations. *Nat. Methods* **2015**, *13*, 55.
- 58. Sunhwan, J.; Taehoon, K.; G., I. V.; Wonpil, I. Charmm-Gui: A Web-Based Graphical User Interface for Charmm. *J. Comput. Chem.* **2008**, *29*, 1859-1865.
- 59. Seonghoon, K.; Jumin, L.; Sunhwan, J.; L., B. C.; Sun, L. H.; Wonpil, I. Charmm-Gui Ligand Reader and Modeler for Charmm Force Field Generation of Small Molecules. *J. Comput. Chem.* **2017**, *38*, 1879-1886.
- 60. Wang, J.; Wang, W.; Kollman, P. A.; Case, D. A. Automatic Atom Type and Bond Type Perception in Molecular Mechanical Calculations. *Journal of Molecular Graphics and Modelling* **2006**, *25*, 247-260.
- 61. Wang, J. M.; Wolf, R. M.; Caldwell, J. W.; Kollman, P. A.; Case, D. A. Development and Testing of a General Amber Force Field. *J. Comput. Chem.* **2004**, *25*, 1157-1174.
- 62. Jakalian, A.; Jack, D. B.; Bayly, C. I. Fast, Efficient Generation of High-Quality Atomic Charges. AM1-BCC Model: II. Parameterization and Validation. *J. Comput. Chem.* **2002**, *23*, 1623-1641.

- 63. Darden, T.; York, D.; Pedersen, L. Particle Mesh Ewald: An *N*·log(*N*) Method for Ewald Sums in Large Systems. *J. Chem. Phys.* **1993**, *98*, 10089-10092.
- 64. Towns, J.; Cockerill, T.; Dahan, M.; Foster, I.; Gaither, K.; Grimshaw, A.; Hazlewood, V.; Lathrop, S.; Lifka, D.; Peterson, G. D.; Roskies, R.; Scott, J. R.; Wilkins-Diehr, N. Xsede: Accelerating Scientific Discovery. *Computing in Science & Engineering* **2014**, *16*, 62-74.
- 65. Frisch, M. J.; Trucks, G. W.; Schlegel, H. B.; Scuseria, G. E.; Robb, M. A.; Cheeseman, J. R.; Scalmani, G.; Barone, V.; Mennucci, B.; Petersson, G. A.; Nakatsuji, H.; Caricato, M. L., X.; ; Hratchian, H. P.; Izmaylov, A. F.; Bloino, J.; Zheng, G.; Sonnenberg, J. L.; Hada, M.; Ehara, M.; Toyota, K., et al. *Gaussian 09*, Gaussian, Inc.: Wallingford CT, 2009.
- Varga, K.; Tannir, S.; Haynie, B. E.; Leonard, B. M.; Dzyuba, S. V.; Kubelka, J.; Balaz, M. CdSe Quantum Dots Functionalized with Chiral, Thiol-Free Carboxylic Acids: Unraveling Structural Requirements for Ligand-Induced Chirality. ACS Nano 2017, 11, 9846-9853.

### **Table of Contents Graphic:**

